## PAPER

# Optimization of the carrier concentration in phase-separated half-Heusler compounds

Julia Krez,*[ab] Jennifer Schmitt,[a] G. Jeffrey Snyder,[c] Claudia Felser,[d] Wilfried Hermes[e] and Markus Schwind[e]

Inspired by the promising thermoelectric properties of phase-separated half-Heusler materials, we investigated the influence of electron doping in the n-type $Ti_{0.3-x}Zr_{0.35}Hf_{0.35}NiSn$ compound. The addition of Nb to this compound led to a significant increase in its electrical conductivity, and shifted the maximum Seebeck coefficient to higher temperatures owing to the suppression of intrinsic carriers. This resulted in an enhancement of both the power factor $\alpha^2\sigma$ and figure of merit, $zT$. The applicability of an average effective mass model revealed the optimized electron properties for samples containing Nb. There is evidence in the literature that the average effective mass model is suitable for estimating the optimized carrier concentration of thermoelectric n-type half-Heusler compounds.

## Introduction

The world energy problem requires a reduction of energy consumption as well as extension of the current research in sustainable energy sources. This need has generated a high interest in the field of thermoelectricity as thermoelectric (TE) materials offer the possibility of directly converting waste heat into usable energy. Besides space applications, this solid-state technology has been intensely investigated for use in the automotive industry.[1,2] Nowadays, different TE materials are used for operation in various temperature ranges, depending on the desired application.[3,4] For example, $Bi_2Te_3$ is the most used TE material for room temperature applications and PbTe for devices operating in a moderate temperature range ($T = 500$–800 K).[5,6] However, Te is rare, and it is questionable whether Pb and Bi are environmentally friendly. Therefore, recent research has focused on abundantly available TE materials that could be used in a high temperature range.

Since the early nineties, theoretical predictions by *Dresselhaus* and *Slack* have driven the efforts toward the development of highly efficient TE materials possessing nanostructures or nanoinclusions, leading to a decisive reduction in their thermal conductivities.[6–9] However, it is doubtful if the criteria of reproducibility and thermal stability can be fulfilled for these nanostructured materials. Therefore, another approach is required to achieve low thermal conductivities. Half-Heusler (HH) compounds comply with many of the requirements for TE applications at high temperatures.[10] The used materials are environmentally friendly and earth abundant. Due to their high thermal stability and power factors, HH compounds have already generated significant interest.[6] The improvement in TE performance is mainly due to the reduction in thermal conductivity caused by an intrinsic phase separation.[11–14] This concept provides a good starting strategy for the improvement of TE efficiency in HH materials. Thus, the phase-separated n-type XNiSn-based complex HH compounds have been intensively investigated in the recent past.[5,11–13] An intrinsic phase separation can be observed in most of the $Ti_xZr_yHf_zNiSn$-based complex HH compounds, while the dendritic microstructure can be retained even under cycling conditions.[15]

A suitable benchmark for researchers in the classification of TE efficiencies of different materials is the dimensionless figure of merit, $zT$. To attain superior material performance, an inevitable compromise has to be made between the Seebeck coefficient and the electrical conductivity. As mentioned before, optimization can be achieved by a reduction of the lattice thermal conductivity *via* high phonon scattering at point defects or interfaces.[5,16] Another approach in enhancing the electronic properties is to take advantage of the prediction of the optimum value to control the carrier concentration. By carefully manipulating the carrier concentration in the case of $Bi_2Te_3$, Snyder *et al.* were able to show that overall performance could be improved.[17]

Various reports have revealed the successful reduction of thermal conductivity in phase-separated HH materials. A further enhancement in the TE performance in HH compounds can be achieved *via* electronic doping of the Sn position, resulting in high $zT$ values up to 1.5 at 700 K.[12,18] In general

*[a]Institute for Inorganic and Analytical Chemistry, Johannes Gutenberg University, Staudingerweg 9, D-55099 Mainz, Germany. E-mail: krez@uni-mainz.de*

*[b]Graduate School for Excellence Materials Science in Mainz, Johannes Gutenberg University Mainz, Staudingerweg 9, D-55128 Mainz, Germany*

*[c]Materials Science, California Institute of Technology, 1200 E. California Blvd, Pasadena, California, 91125, USA*

*[d]Max Planck Institute for Chemical Physics of Solids, D-01187 Dresden, Germany*

*[e]BASF SE, Carl-Bosch-Str. 38, D-67056 Ludwigshafen, Germany*

This journal is © The Royal Society of Chemistry 2014

*J. Mater. Chem. A*, 2014, **2**, 13513–13518 | **13513**

XNiSn-based HH materials exhibit small band gaps of about 0.15–0.23 eV,[19] where minority carriers can be easily excited at higher temperatures. Bipolar conduction has an adverse impact on the TE performance, resulting in the reduction of the Seebeck coefficient and an increase in the thermal conductivity at higher temperatures. Thus, in order to prevent a decline in TE performance, it is crucial to suppress this bipolar conduction, which can be realized by electronic doping.[20] In this work we investigate the influence of Nb in the $Ti_{0.3-x}Nb_xZr_{0.35}Hf_{0.35}NiSn$ ($x = 0$–0.05) system, where an intrinsic phase separation is observed as a result of the intermixing of Ti, Zr and Hf. The TE properties were investigated up to 850 K. Because of the introduction of Nb, it is possible to suppress the minority carrier contribution, leading to an improvement in the TE performance of the n-type $Ti_{0.3}Zr_{0.35}Hf_{0.35}NiSn$ material. The electrical conductivity is enhanced by introduction of Nb inclusions, increasing the power factor and figure of merit. The optimum carrier concentration for the n-type $Ti_{0.3}Zr_{0.35}Hf_{0.35}NiS$ system was investigated within the framework of an average effective mass model, and compared with those of other Nb-substituted HH compounds. The applied theory supports the assumption that for both phases the conduction of the majority electrons takes place in the conduction bands and that, within a particular temperature range, the influence of the minority carriers can be neglected. From this transport theory, we were able to estimate the optimum carrier concentration and its correlated maximum value for $zT$.

## Experimental

$Ti_{0.3-x}Nb_xZr_{0.35}Hf_{0.35}NiSn$ samples ($x = 0$, 0.01, 0.03 and 0.05) were prepared by arc melting of stoichiometric amounts of Ti (99.9%), Zr (99.9%), Hf (99.9%), Nb (99.9%), Ni (99.99%) and Sn (99.99%) under argon atmosphere. To ensure homogeneity, the samples were crushed and re-melted three times. The cast samples were subsequently annealed in evacuated quartz tubes at 1273 K for 7 days to improve their crystalline order, followed by quenching in ice water. Their crystal structure was analyzed by powder X-ray diffraction (PXRD) at room temperature with a Huber Guinier Kamera G670 using Cu $K\alpha_1$ radiation and a Ge(111) monochromator. The lattice parameter was determined using $LaB_6$ as an internal standard. The chemical compositions of the obtained samples, with an accuracy of approximately 0.5–0.3 at%, were examined by scanning electron microscopy (SEM) using the Philips XL30 scanning electron microscope. Quantitative electron probe microanalysis (EPMA) of the phases was carried out with a voltage of 25 kV with a wavelength dispersive X-ray analyzer (Phoenix V 5.29, EDAX). The electrical conductivity $\sigma$ and the Seebeck coefficient $\alpha$ were measured simultaneously with a Linseis LSR-3 system in a helium gas atmosphere from room temperature to about 900 K. The thermal conductivity $\kappa$ was evaluated as a product of the thermal diffusivity $D$, heat capacity $c_p$ and measured density $\rho$. The thermal diffusivity $D$ was measured by a laser flash method with a Netzsch LFA 457 apparatus. All samples were coated with a thin layer of graphite to minimize the reflectivity of the sample surface. The heat capacity $c_p$ was measured by differential scanning calorimetry

(DSC) with a Netzsch STA 449 instrument. The density was determined *via* a geometrical method by measuring the weight and dimension of the rectangular bars, and was found to be $\sim$8.4 g cm$^{-3}$ (>98% of the theoretical density) for all samples. The Hall coefficient, $R_H$, Hall carrier concentration, $n_H$, and Hall mobility $\mu_H$ were measured in a $\pm 2$ T magnetic field using pressed niobium contacts.[21] The Hall carrier concentration, $n_H$ was calculated as follows:

$$n_H = -\frac{1}{eR_H} \tag{1}$$

where $R_H$ is the Hall coefficient and $e$ is the electron charge. The Hall mobility $\mu_H$ was calculated from the Hall coefficient and electrical conductivity using equation:

$$\mu_H = R_H\sigma. \tag{2}$$

## Results and discussion

### Crystal structure

The crystalline structure in the $Ti_{0.3-x}Nb_xZr_{0.35}Hf_{0.35}NiSn$ ($x = 0$, 0.01, 0.03 and 0.05) system was verified by powder X-ray diffraction (PXRD) measurements using $LaB_6$ as internal standard. The obtained X-ray patterns agree with the cubic $C1_b$ structure ($F\bar{4}3m$) discussed in the literature.[22] In all samples, a splitting of the Bragg reflection peaks (Fig. 1a) could be found because of the coexistence of two HH phases (HH1 and HH2) due to an intrinsic phase separation in the $Ti_{0.3}Zr_{0.35}Hf_{0.35}NiSn$ system.[14,23] The lattice parameter $a$ of the Zr–Hf-rich phase (HH1) and the Ti-rich phase (HH2) was estimated by a refinement of the peak position using $LaB_6$ as an internal standard and found to be 6.068 Å, and 6.001 Å, respectively. With increasing Nb content, a decrease in the lattice parameter could be observed. The radii of Ti (144 pm) and Nb (143 pm) are almost equal, thus a successful substitution should cause no significant change in the unit cell. Therefore, the decrease in the lattice parameter results from the decreased Ti content in the HH system, where no substitution with Nb can be observed. Muta *et al.* investigated the impact of Nb substitution on the TE properties of XNiSn (X = Ti and Zr).[21] However, the effect of the Nb substitution on the lattice constant was not discussed. In this study, the electron probe microanalysis (EPMA) of the samples revealed a Zr–Hf rich main phase (HH1), which was dendritically interlaced by a Ti-rich phase (HH2)[14,22] along with homogeneously distributed Nb metallic inclusions. In order to emphasize the presence of Nb, the samples were etched with a $HCl–HNO_3–HF–H_2O$ solution as shown in Fig. 1b. The data from EMPA (Fig. 1c) and PXRD confirm that Nb was not completely substituted for Ti, since Nb has the highest melting point (2740 K) of all elements within the compound.

### Transport properties

The results of the study of electrical conductivity $\sigma$ of the $Ti_{0.3-x}Nb_xZr_{0.35}Hf_{0.35}NiSn$ ($x = 0$, 0.01, 0.03 and 0.05) is shown in Fig. 2. The parent compound, $Ti_{0.3}Zr_{0.35}Hf_{0.35}NiSn$, exhibits

13514 | *J. Mater. Chem. A*, 2014, **2**, 13513–13518

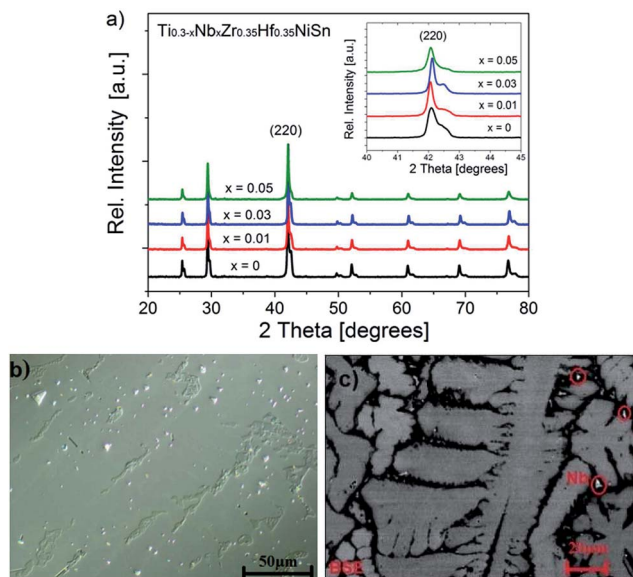This journal is © The Royal Society of Chemistry 2014

Fig. 1 (a) XRD pattern with the inset showing the (220)-reflex peak as an example of the peak splitting due to the intrinsic phase separation into a Zr–Hf-rich phase (HH1) and a Ti-rich phase (HH2). (b) Light microscope image of the $Ti_{0.25}Nb_{0.05}Zr_{0.35}Hf_{0.35}NiSn$ etched with a $HCl–HNO_3–HF–H_2O$ solution to highlight the metallic Nb inclusions. (c) BSE image of the phase-separated microstructure in the $Ti_{0.3}Zr_{0.35}Hf_{0.35}NiSn$ HH system, consisting of the Zr–Hf-rich main phase (HH1, grey) and the dendritically interlaced Ti-rich phase (HH2, black). The red circles highlight the Nb inclusions.
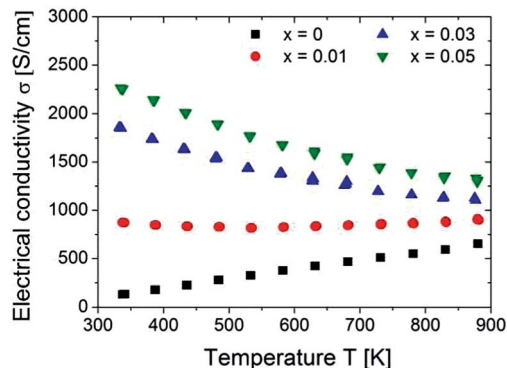


Fig. 2 The temperature dependence of the electrical conductivity $\sigma$. in the $Ti_{0.3-x}Nb_xZr_{0.35}Hf_{0.35}NiSn$ ($x = 0, 0.01, 0.03$ and $0.05$) system from 300 to 900 K. The electrical conductivity becomes more metallic with increasing Nb concentration.

an intrinsically semiconducting behavior, as $\sigma$ increases with temperature. The addition of Nb drastically increases the value of $\sigma$ at room temperature and facilitates the transition from intrinsically conducting to a metal-like behavior. The increase of the electrical conductivity with the addition of Nb is compensated by a systematic decrease of the room temperature Seebeck coefficient $\alpha$.

The temperature dependence of $\alpha$ for all samples exemplified in Fig. 3, revealed negative values over the whole temperature range, which indicated that electrons are the majority
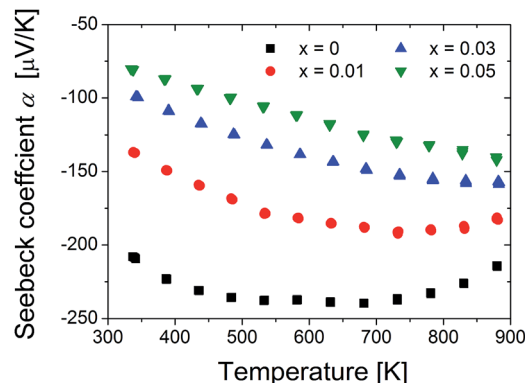


Fig. 3 The temperature dependence of the Seebeck coefficient $\alpha$ in the $Ti_{0.3-x}Nb_xZr_{0.35}Hf_{0.35}NiSn$ ($x = 0, 0.01, 0.03$ and $0.05$) system from 300 to 900 K.

carriers. The maximum Seebeck coefficient of $-240\ \mu V\ K^{-1}$ was measured for the parent compound $Ti_{0.3}Zr_{0.35}Hf_{0.35}NiSn$. The metallic inclusions were responsible for attaining the maximum Seebeck coefficient at higher temperatures than before. Caused by the suppression of the minority carrier conduction above the usual temperature of around 600 K.[10]

While, $\sigma$ increased with increasing Nb concentration, the absolute value of the Seebeck coefficient was reduced, though not at a similarly fast rate, leading to an improvement of the power factor (Fig. 4). The power factors were calculated from the relation PF = $\alpha^2\sigma$ and are shown in Fig. 2c. By comparing the samples with Nb content with the parent compound, it can be seen that the ones with metal inclusions exhibit a significant enhancement of the power factor. The highest power factor was attained in the sample with 5% Nb content.

Fig. 5 shows the temperature dependence of the thermal conductivity ($\kappa = \kappa_e + \kappa_l$) with increasing Nb content. According to the Wiedemann–Franz Law:

$$\kappa_e = L\sigma T = ne\mu LT \qquad (3)$$

where $L$ is the Lorenz number, and $\kappa_e$ is proportional to $\sigma$. Therefore, the observed increase of the total thermal conductivity can only be explained by an increase in $\kappa_e$, induced by the
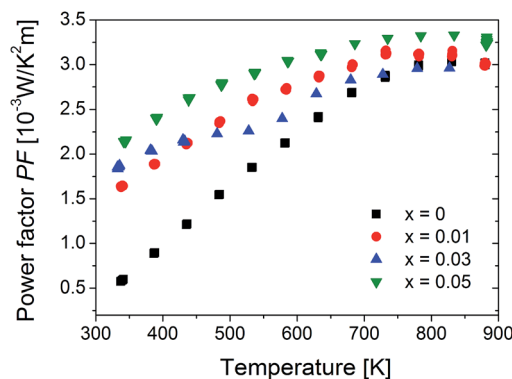


Fig. 4 The temperature dependence of power factor $\alpha^2\sigma$ in the $Ti_{0.3-x}Nb_xZr_{0.35}Hf_{0.35}NiSn$ ($x = 0, 0.01, 0.03$ and $0.05$) system.
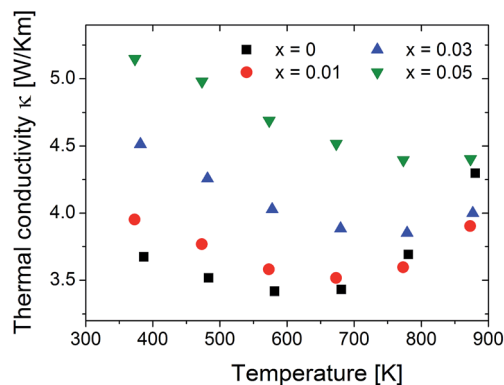
This journal is © The Royal Society of Chemistry 2014

J. Mater. Chem. A, 2014, **2**, 13513–13518 | **13515**

Fig. 5 The temperature dependence of the thermal conductivity $\kappa$, in the Ti$_{0.3-x}$Nb$_x$Zr$_{0.35}$Hf$_{0.35}$NiSn ($x = 0$, 0.01, 0.03 and 0.05) system from 300 to 900 K.
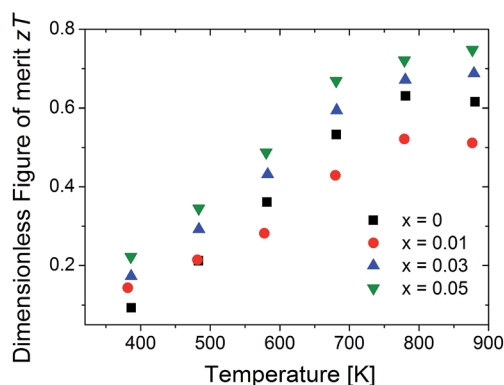


Fig. 6 Temperature dependence of the dimensionless figure of merit $zT$ in the Ti$_{0.3-x}$Nb$_x$Zr$_{0.35}$Hf$_{0.35}$NiSn ($x = 0$, 0.01, 0.03 and 0.05) system from 300 to 900 K.

metal inclusions observed in the system. The influence of bipolar conduction, which is derived from the thermal excitation of minority carriers, can only be observed in the parent compound Ti$_{0.3}$Zr$_{0.35}$Hf$_{0.35}$NiSn. The aforementioned electron doping of Nb suppresses bipolar conduction, shifting it to higher temperatures.

The figure of merit, $zT$, was also enhanced with Nb addition (Fig. 6). This is an important point, as most improvements in HH compounds are achieved as a result of a drastic reduction in the lattice thermal conductivity. The metal inclusions influence the transport properties strongly because of the introduction of electrons into the HH system, the factor responsible for the significant increase in the electrical conductivity $\sigma$. The observed decrease in the absolute Seebeck coefficient $\alpha$ does not impact the TE efficiency as dramatically as the increase in the electrical conductivity does. In this study, the highest $zT$ obtained was for a Nb concentration of 5%.

### Hall measurements

Fig. 7a shows the Hall carrier concentration of the Ti$_{0.3-x}$Nb$_x$Zr$_{0.35}$Hf$_{0.35}$NiSn system, which increased significantly with an increase in the Nb concentration. For samples with high
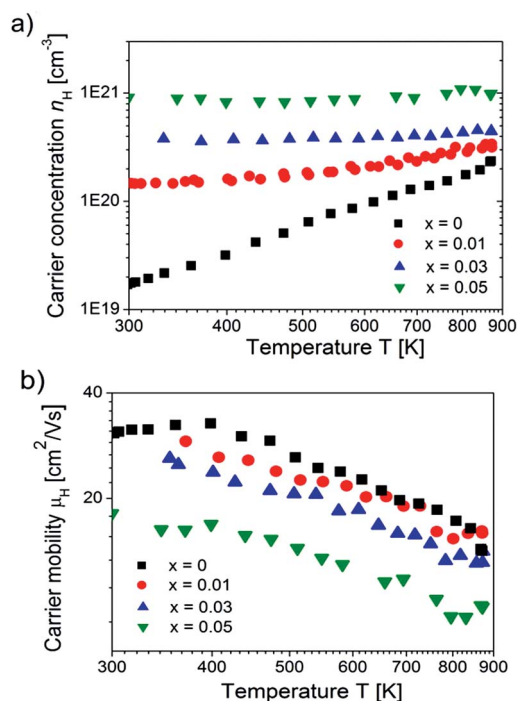


Fig. 7 Shown are the temperature dependence of (a) the Hall carrier concentration $n_H$ and (b) the Hall mobility $\mu_H$ for the Ti$_{0.3-x}$Nb$_x$Zr$_{0.35}$Hf$_{0.35}$NiSn ($x = 0$, 0.01, 0.03 and 0.05) system from 300 to 900 K.

Nb content, it could be observed that the carrier concentration remained constant and no intrinsic excitation occurred at high temperatures. The Hall mobility, $\mu_H$ (Fig. 7b) decreased with increasing Nb concentration, which may be caused by the scattering of the charge carriers as a result of the additional metal inclusions. The variation in mobility with temperature can be described by a power law equation: $\mu \propto T^{-\nu}$, where the value of $\nu$ is an indicator of the most dominant scattering mechanism in the system. For phase-separated HH compounds, Xie et al. were able to show that the major mechanism is alloy scattering.[24]

The experimental transport data of Ti$_{0.3-x}$Nb$_x$Zr$_{0.35}$Hf$_{0.35}$NiSn ($x = 0$, 0.01, 0.03 and 0.05) were analyzed using an average effective mass model. To obtain a mean value for the effective mass $m^*$, it was assumed that electron conduction occurs only within the conduction band for each HH phase. In this theory, the Seebeck coefficient and carrier concentration can be calculated by:

$$\alpha = \frac{k_B}{e}\left(\frac{(2+\lambda)F_{1+\lambda}(\eta)}{(1+\lambda)F_\lambda(\eta)}\right) - \eta \tag{4}$$

$$n_H = 4\pi\left(\frac{2m^*k_B T}{h^2}\right)^{3/2} F_{1/2} \tag{5}$$

where $F_\lambda(\eta)$ is the Fermi integral:

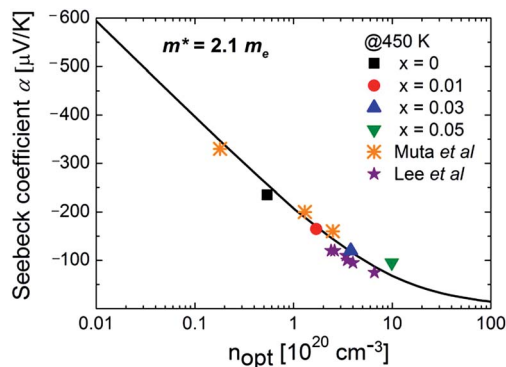$$F_\lambda(\eta) = \int_0^\infty \frac{\xi^\lambda \mathrm{d}\xi}{1 + \exp[\xi - \eta]} \tag{6}$$

13516 | J. Mater. Chem. A, 2014, 2, 13513–13518

This journal is © The Royal Society of Chemistry 2014

Fig. 8   Seebeck coefficient, $\alpha$ vs. carrier concentration together with a comparison of the literature data.[20,26]

$\eta$ is the reduced chemical potential that can be determined from the experimentally measured Seebeck coefficient of each sample at different temperatures according to eqn (4). $k_B$, $e$, $h$, $\lambda$ and $m^*$ are respectively the Boltzmann constant, electron charge, Planck constant, scattering factor, and the density-of-state effective mass. It can be assumed that, in general, the phonon mean free path is limited by acoustic phonon scattering.[25] The Seebeck coefficient derived from the experimental values versus an optimized carrier concentration is given in Fig. 8. For this evaluation, we assumed that the onset of the contribution of minority carriers is above 460 K. Considering this with the calculation from the above mentioned theory, we obtained an average effective mass value of $m^* = 2.1\ m_e$ for both phases. The agreement between the experimental results[20,26] and the theoretical calculation justifies the use of an average effective mass model for the estimation of the effective mass and the prediction of the optimum carrier concentration.

The optimization of $zT$ with carrier concentration was confirmed within the framework of the applied model. From the results of the transport measurements, an average effective
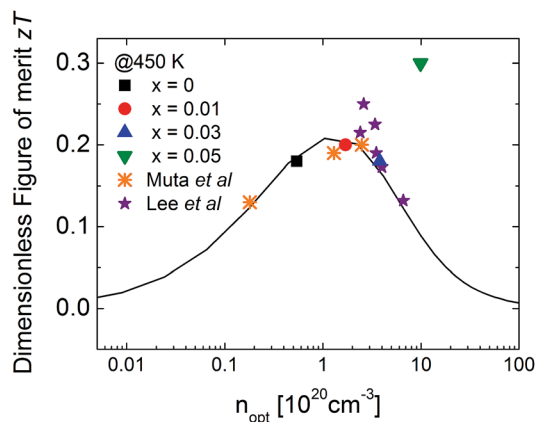
mass model was developed to determine the optimum carrier concentration. Fig. 9 shows that the results obtained are in good agreement with the data presented in the literature.[20,26] The metallic inclusions generate more electrons in the system and therefore influence the electrical conductivity as well as the magnitude of the Seebeck coefficient, resulting in an enhancement of $\alpha^2\sigma$ and an increase of the figure of merit, $zT$.

## Conclusions

The thermally stable phase-separated half-Heusler (HH) compounds exhibit excellent thermoelectric performance.[9] In this study, the influence of Nb on the high temperature thermoelectric properties of $Ti_{0.3-x}Nb_xZr_{0.35}Hf_{0.35}NiSn$ ($x = 0$, 0.01, 0.03 and 0.05) was investigated. Our results confirmed the exceptional performance of the phase-separated HH materials. Nb inclusions are responsible for the significant increase in the electrical conductivity and the shift to higher temperatures for the maximum Seebeck coefficient. Both parameters lead to an enhancement of the power factor and the dimensionless figure of merit. To calculate the optimization of $zT$ with carrier concentration, we used the Boltzmann transport theory. From the results of the transport measurements, an average effective mass of $m^* = 2.1\ m_e$ for both HH phases was calculated, which is in good agreement with the values from the literature.[20,26] These results justify the use of an average effective mass model to describe the carrier transport within the conduction band of these n-type HH compounds.

## Acknowledgements

Fig. 9   The triangles and stars represent the values used from the literature.[20,26] The squares are the obtained values for the $Ti_{0.3-x}Nb_xZr_{0.35}Hf_{0.35}NiSn$ from our measurements. The solid line represents the estimate of the optimized carrier concentration predicted by the average effective mass model, assuming $m^* = 2.1\ m_e$, $\mu_0 = 25$ cm$^2$ V$^{-1}$ s$^{-1}$ and $\kappa_l = 3$ W km$^{-1}$.

## References

1   A. Angrum, NASA and JPL. Voyager the interstellar mission, http://voyager.jpl.nasa.gov/spacecraft/instruments_rtg.html, NAJA, JPL, http://voyager.jpl.nasa.gov/spacecraft/instruments_rtg.html.

2   K. Schierle-Arndt and W. Hermes, Chem. Unserer Zeit, 2013, 47, 92–101.

3   K. Nielsch, J. Bachmann, J. Kimling and H. Böttner, Adv. Energy Mater., 2011, 1, 713–731.

4   L. D. Zhao, S. H. Lo, Y. Zhang, H. Sun, G. Tan, C. Uher, C. Wolverton, V. P. Dravid and M. G. Kanatzidis, Nature, 2014, 508, 373–377.

5   J. R. Sootsman, D. Y. Chung and M. G. Kanatzidis, Angew. Chem., Int. Ed., 2009, 48, 8616–8639.

6   Z. Ren and S. Chen, Mater. Today, 2013, 16, 387–394.

7   L. D. Hicks and M. S. Dresselhaus, Phys. Rev. B: Condens. Matter Mater. Phys., 1993, 47, 12727–12731.

8   G. Slack, CRC Handbook of Thermoelectrics, 1995.

9   Y. Ma, R. Heijl and A. E. C. Palmqvist, J. Mater. Sci., 2013, 48, 2767–2778.

10 W. Liu, X. Yan, G. Chen and Z. Ren, *Nano Energy*, 2012, **1**, 42–56.

11 T. Graf, C. Felser and S. Parkin, *Prog. Solid State Chem.*, 2011, **3**, 1–50.

12 M. Schwall and B. Balke, *Phys. Chem. Chem. Phys.*, 2013, **15**, 1868–1872.

13 C. Uher, J. Yang, S. Hu, D. T. Morelli and G. P. Meisner, *Phys. Rev. B: Condens. Matter Mater. Phys.*, 1999, **59**, 8615–8621.

14 N. Shutoh, S. Sakurada, N. Kondo and N. Takezawa, US patent 0037199A1, 16, Febrauary 2012.

15 J. Krez, B. Balke, C. Felser, W. Hermes and M. Schwind, submitted.

16 J. R. Sootsman, D. Y. Chung and M. G. Kanatzidis, *Angew. Chem., Int. Ed.*, 2009, **48**, 8616–8639.

17 G. J. Snyder and E. S. Toberer, *Nat. Mater.*, 2008, 7, 105–114.

18 S. Sakurada and N. Shutoh, *Appl. Phys. Lett.*, 2005, **86**, 082105–0821053.

19 F. G. Aliev, N. B. Brandt, V. V. Moshchalkov, V. V. Kozyrkov, R. V. Skolozdra and A. I. Belogorokhov, *Z. Phys. B: Condens. Matter*, 1998, **75**, 167–171.

20 L. D. Zhao, H. J. Wu, S. Q. Hao, C. I. Wu, X. Y. Zhou, K. Biswas, J. Q. He, T. P. Hogan, C. Uher, C. Wolverton, V. P. Dravid and M. G. Kanatzidis, *Energy Environ. Sci.*, 2013, **6**, 3346–3355.

21 K. A. Borup, E. S. Toberer, L. D. Zoltan, G. Nakatsukasa, M. Errico, J.-P. Fleural, B. B. Iversen and G. J. Snyder, *Rev. Sci. Instrum.*, 2012, **83**, 123902–123907.

22 H. Muta, T. Kanemitsu, K. Kurosaki and S. Yamanaka, *J. Alloys Compd.*, 2009, **469**, 50–55.

23 S. Populoh, M. H. Aguirre, O. C. Brunko, K. Galazka, X. Lu and A. Weidenkaff, *Scr. Mater.*, 2012, **66**, 1073–1076.

24 H. Xie, H. Weng, Y. Pei, C. Fu, Y. Liu, G. J. Snyder, X. Zhao and T. Zhu, *Adv. Funct. Mater.*, 2013, **23**, 5123–5218.

25 E. S. Toberer, A. Zevalkink and G. J. Synder, *J. Mater. Chem.*, 2011, **21**, 15843–15852.

26 P.-J. Lee and L.-S. Chao, *J. Alloys Compd.*, 2010, **504**, 192–196.